Measuring the Folding Transition Time of Single RNA Molecules

Tae-Hee Lee,* Lisa J. Lapidus,* Wei Zhao,* Kevin J. Travers,† Daniel Herschlag,† and Steven Chu*‡
*Department of Physics and Applied Physics, Stanford University, Stanford, California; †Department of Biochemistry, Stanford University School of Medicine, Stanford, California; and ‡Lawrence Berkeley National Laboratory, Department of Physics and Molecular and Cell Biology, University of California-Berkeley, Berkeley, California

ABSTRACT We describe a new, time-apertured photon correlation method for resolving the transition time between two states of RNA in folding—i.e., the time of the transition between states rather than the time spent in each state. Single molecule fluorescence resonance energy transfer and fluorescence correlation spectroscopy are used to obtain these measurements. Individual RNA molecules are labeled with fluorophores such as Cy3 and Cy5. Those molecules are then immobilized on a surface and observed for many seconds during which time the molecules spontaneously switch between two conformational states with different levels of flourescence resonance energy transfer efficiency. Single photons are counted from each fluorophore and cross correlated in a small window around a transition. The average of over 1000 cross correlations can be fit to a polynomial, which can determine transition times as short as the average photon emission interval. We applied the method to the P4–P6 domain of the *Tetrahymena* group I self-splicing intron to yield the folding transition time of 240 μs. The unfolding time is found to be too short to measure with this method.

INTRODUCTION

Single molecule fluorescence resonance energy transfer (SM FRET) is a powerful tool to study the structural dynamics of many biological molecules (1–4). This method is capable of yielding subpopulation dynamics with high signal/noise and requires very small numbers of molecules compared to bulk methods. There have been many measurements of single molecule structural dynamics ~1 ms or longer using SM FRET (5–8), but measurements with higher time resolution have been elusive due to the rate of photon emission from the commonly used fluorophores (typically 5 kHz). Fluorescence correlation spectroscopy (FCS), which is sensitive to transient fluctuations in fluorescence intensity (9–14), can extend the time resolution down to the average arrival time of individual photons (5,15). Structural dynamics of only a few biological systems have been probed so far by SM FRET and FCS, but these experiments have only measured the residence times of interconverting states, not the transition time (5,7,16).

In this article we introduce a new method to measure the folding transition time of a single RNA molecule using FCS and SM FRET. By filtering and correlating only the relevant photons surrounding the folding transitions, fast dynamics on the timescale of the average photon arrival interval can be measured by observing ~1000 transitions under typical SM FRET experimental conditions.

The experimental system for this study comprises a fragment of the group I self-splicing intron from *Tetrahymena* (17,18). The fragment, the P4–P6 domain (19–23), has been shown to fold in isolation upon the addition of divalent ions such as magnesium (21,24,25). For this study we have labeled the ends of the P4 and P6 helices with the fluorophores Cy3 and Cy5 (Fig. 1 *a*). Cy3 acts as a donor for Cy5 such that the observed intensities from each dye can be compared as

$$FRET = \frac{I_a}{I_a + I_d} = \frac{1}{1 + (r/R_0)^6}, \quad (1)$$

where I_a and I_d are the Cy5 and Cy3 intensities, respectively, r is the distance between the fluorophores, and R_0 is a characteristic distance at which FRET = 0.5 and is dependent on a number of intrinsic parameters of the fluorophores (26). For these fluorophores, R_0 is ~5 nm.

MATERIALS AND METHODS

Sample preparation and labeling

The P4–P6 domain of the *Tetrahymena* group I intron was used as the system to follow folding dynamics. The RNA molecule was prepared by ligation reactions mediated by DNA splints (27,28). Five RNA fragments and four DNA splints were used to construct the RNA molecule of nucleotides 102–261 of the *Tetrahymena* group I intron. The first two nucleotides at its 5′-end were replaced with guanosine residues to allow in vitro transcription by T7 RNA polymerase. The five RNA fragments used correspond to the sequences: 102–148, 163–234, 250–261, 149–162, and 235–249 (the first three were prepared from in vitro transcription, and the last two were purchased from Dharmacon, Lafayette, CO). The final construct also has a 26-nucleotide tether at the 3′-end for surface immobilization (4). This tether sequence is ACCAAAAUCAACCUAAAACUUACACA. The DNA template for the transcription was obtained by the polymerase chain reaction from wild-type *Tetrahymena* group I intron L-21 ScaI plasmid. The DNA splints were complementary to nucleotides 162–129, 261–235, 261–215, and 181–137. Nucleotides U155 and U241 were replaced with 5-amino-allyl uridine. The oligomers containing those two nucleotides—U155 and U241—were then labeled with Cy5 and Cy3, respectively. T4 DNA ligase was used to join the RNA pieces to form P4-P6, and a typical ligation reaction protocol was followed (annealing for 3 min at 95°C, cooling for 1–2 h, and then the ligation reaction for several hours to

Submitted August 7, 2006, and accepted for publication January 18, 2007.
Address reprint requests to Tae-Hee Lee, E-mail: leeth@stanford.edu.

0006-3495/07/05/3275/09 $2.00
doi: 10.1529/biophysj.106.094623

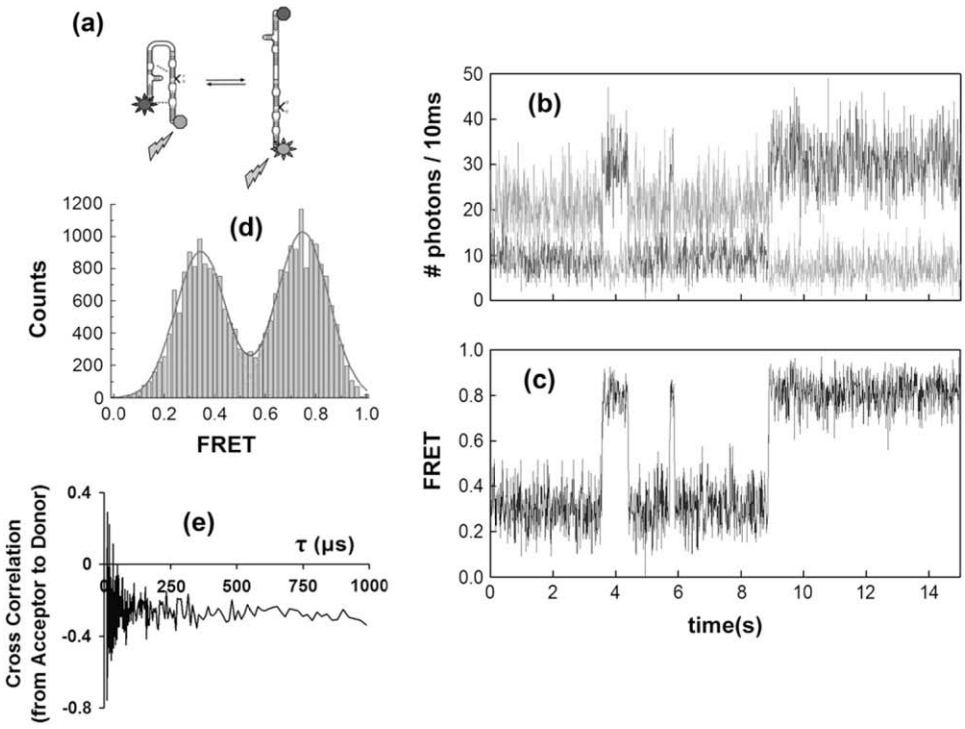

FIGURE 1 (*a*) Structure of the P4–P6 molecule labeled with Cy3 (*light gray*) and Cy5 (*dark gray*). At the conditions of these experiments the molecule spends about half the time in the folded and unfolded states corresponding to high FRET and low FRET, respectively. (*b*) Typical time trace of single molecule FRET. The light gray line is the number of photons detected (per 10 ms) in the Cy3 channel and the dark gray line is the number of photons detected in the Cy5 channel. (*c*) Fluorescence resonance energy transfer efficiency (FRET) given by Eq. 1 of the data in panel *b*. (*d*) Histogram of FRET efficiency from 15 representative molecules. The two Gaussian peaks yield a low FRET state, $A' = 0.344$, and a high FRET state, $B' = 0.747$ ($\Delta FRET = 0.403$). (*e*) Averaged cross correlation from 1133 folding transitions.

overnight). Control digestion experiments revealed ~20% aberrant P4–P6 with incorrect ligation junctions (K. Travers and W. Zhao, unpublished results); although this material could show different folding behavior from P4–P6 with the all-native sequence, no differences in the equilibrium population of folded and unfolded molecules for this construct relative to the native molecule transcribed as a single piece was detected as a function of Mg^{2+} concentration (K. Travers and W. Zhao, unpublished results).

Surface immobilization

Fluorescently labeled molecules were immobilized on a glass coverslip using the biotin-streptavidin-biotin system described elsewhere (5). The buffer used during experiments contained 20 mM NaMOPS, pH 7.0, 10 mM NaCl, and 0.5 mM $MgCl_2$ and was deoxygenated using a combination of glucose oxidase, catalase, and β-mercaptoethanol. Chloramphenicol (1 mM) was also added to prevent Cy5 blinking.

Instrument

The instrument for observing SM FRET has been described elsewhere (5). Briefly, the immobilized molecules are observed with a scanning confocal microscope, which can resolve dozens of individual molecules in a 100-μm^2 area. The Cy3 dye is excited with the second harmonic of a CW Nd:YAG laser (CrystaLaser GCL-532-L; Reno, NV) focused to a 0.2-μm spot with an objective (Olympus APO 60× 1.45 NA; Tokyo, Japan). Laser excitation power is continuously adjusted to achieve a constant 5 kHz photon emission rate from a single Cy3. The immobilized molecules are moved over the laser focus with a piezoelectric scanner (Mad City Labs NanoBio2; Madison, WI). Fluorescence captured with the same objective is focused on a pinhole to remove stray light and split into two spectra using a dichroic mirror such that the Cy3 fluorescence is focused on one detector and the Cy5 fluorescence is focused on the second detector (Perkin Elmer SPCM-AQR-16; Foster City, CA). The arrival time of each photon detected is stored on a computer with ~100 ns time resolution through a digital pulse counter (National Instruments 6602 counter; Austin, TX). Each molecule was observed for 20 s during which time the Cy5 typically photobleaches.

RESULTS

Fig. 1 *b* shows the time trace of a single molecule observed with SM FRET. The photon arrival times were binned into 10-ms windows for this figure. The ionic conditions were chosen such that each molecule spends about half the time in low FRET (unfolded) state and half the time in the high FRET (folded) state to maximize the number of transitions observed. Fig. 1 *d* shows a histogram of FRET values for 15 representative molecules among 1133 studied. The average time between transitions is 3 s, and on the timescale of bin width, the transition time between high and low FRET states is instantaneous. The vast majority of the photons collected are from molecules in either of the two states, folded or unfolded. Thus, their inclusion in the correlation would merely mask the small number of photons emitted during a folding transition.

The major result of this article is that we can measure the timescale of intermediate changes of RNA folding/unfolding that is as short as the average photon arrival interval from FRET. This measurement is done by time-aperturing the photon stream from each fluorophore. Each single molecule trace was parsed to only include photons within 10 ms of a transition. The transitions were found automatically by searching for spikes in the derivative of the FRET trace. However, each identified transition was also reviewed and approved by hand. For a transition that lasts 200 μs, the probability of more than one pair of photons being emitted during that period is only 26%.

Because the donor fluorescence is anticorrelated with the acceptor fluorescence, the autocorrelation of either channel

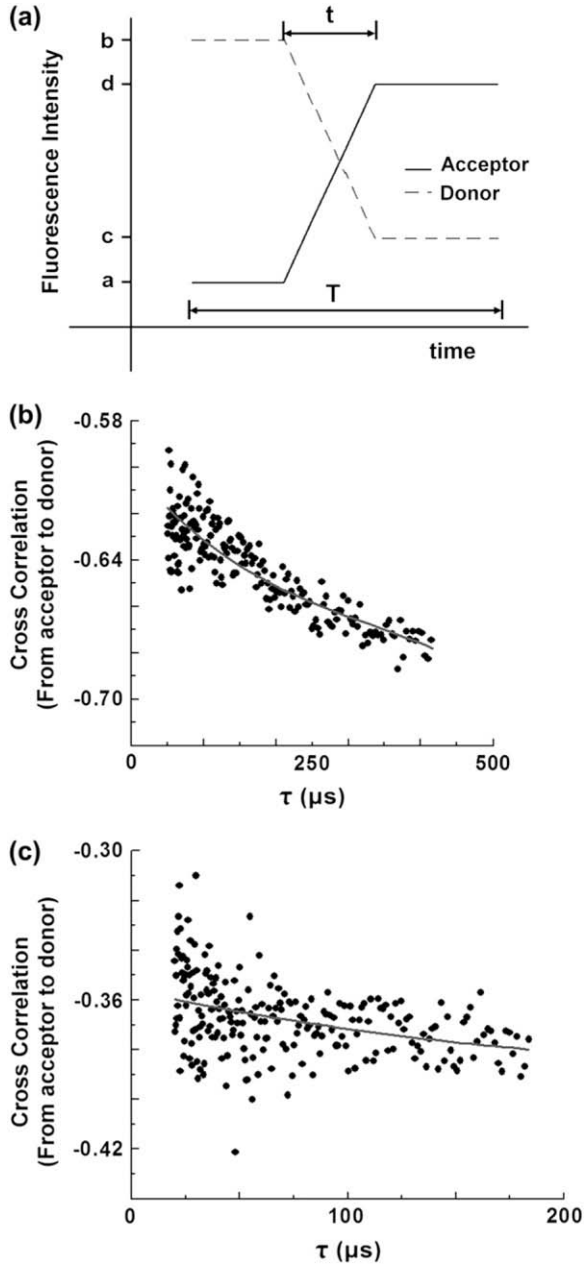

FIGURE 2 A model of SM FRET in RNA folding and photon correlations from simulated folding events. (*a*) A model of SM FRET signal changes during RNA folding. The FRET pair is assumed to be attached to an RNA molecule such that FRET efficiency increases as it folds; *a*, *b*, *c*, and *d* = fluorescence intensities, *t* = folding time, *T* = data window size for correlation. (*b*) An averaged cross correlation of simulated photons from 10 folding transitions. Fluorescence photons from donor within a time window *T* were generated in 100-ns resolution to follow the Poisson statistics using a random number generator. According to the FRET efficiency defined as in panel *a*, donor photons are transferred to the acceptor. Single photons from donor and acceptor were correlated as explained in the text. Individual correlation curves from individual traces were then averaged. Simulation conditions are 500 kHz photon emission rate, $A = 0.1$, $B = 0.9$, $t = 400$ μs, and $T = 5$ ms, where *A* and *B* are the FRET efficiencies before and after the folding transition. Solid line is a third-order polynomial fit to the correlation (with the fixed first order coefficient). Equation 5 was used to determine the folding transition time, *t*. The folding transition time was measured to be 370 μs from the intercept of Eq. 5. (*c*) An averaged cross correlation of simulated photons from 1000 folding transitions. Simulation conditions are 50 kHz photon emission rate, $A = 0.2$, $B = 0.8$, $t = 200$ μs, and $T = 10$ ms. Solid line is a third-order polynomial fit to the correlation (with the fixed first order coefficient). The folding transition time *t* was measured to be 180 μs from the intercept of Eq. 5. Fitted *t* estimates the simulated *t* reproducibly within 20% error for 200, 400, 600, and 800 μs from the averaged 1000 transitions per each case with 50 kHz photon emission rate to confirm the validity of the simulation.

should yield the same information as the cross correlation between the two channels. However, the cross correlation is much less sensitive to channel-specific dynamics such as dye isomerism (29) or autofluorescence of optical filters. The cross correlation for photons detected in the acceptor channel to photons detected in the donor channel is given by

$$CC(\tau) = \frac{\langle \delta I_a(x)\delta I_d(x+\tau)\rangle}{\langle I_a(x)\rangle\langle I_d(x)\rangle} = \frac{\langle I_a(x)I_d(x+\tau)\rangle}{\langle I_a(x)\rangle\langle I_d(x)\rangle} - 1$$
$$\delta I_a(x) = I_a(x) - \langle I_a(x)\rangle, \quad \delta I_d(x) = I_d(x) - \langle I_d(x)\rangle, \quad (2)$$

where $I_a(x)$ is acceptor intensity at time x and $I_d(x)$ is donor intensity at time x.

An equivalent and computationally inexpensive method for calculating the cross correlation between individual photons is to make a histogram of times between photons from the acceptor channel and the donor channel. Fig. 1 *e* shows the averaged cross correlation from 1133 folding transitions. We model the change in FRET through the folding transition as shown in Fig. 2 *a*. This or an analogous assumption about the nature of the transition is required to build an analytical framework with which one uses cross correlations to extract transition times. The model assumes that the transition from low to high FRET state (i.e., the folding transition) takes place linearly during time *t* (Fig. 2 *a*). Therefore the cross correlation is given by

$$\begin{aligned} CC_{\text{acceptor}\to\text{donor}}(\tau,t) &= \frac{\langle \delta I_a(x,t)\delta I_d(x+\tau,t)\rangle}{\langle I_a(x,t)\rangle\langle I_d(x,t)\rangle} \\ &= \frac{\langle I_a(x,t)I_d(x+\tau,t)\rangle}{\langle I_a(x,t)\rangle\langle I_d(x,t)\rangle} - 1 \\ &= \frac{\dfrac{\int_0^{T-\tau} I_a(x,t)I_a(x,t)dx}{(T-\tau)}}{\dfrac{(a+d)}{2}\dfrac{(b+c)}{2}} - 1, \end{aligned} \quad (3)$$

where T is the size of the window and τ is the time domain, $I_a(x,t)$ is acceptor intensity profile along time x with transition time t, $I_d(x,t)$ is donor intensity profile along time x with transition time t, a, and b are the acceptor and donor intensities in unfolded (low FRET) state, respectively, and d and c are the acceptor and donor intensities in folded (high FRET) state, respectively (Fig. 2 *a*). Making a further assumption that the transition takes place in the middle of the

transition window (Fig. 2 *a*), the profiles of donor and acceptor intensities, $I_d(x,t)$ and $I_a(x,t)$, respectively, are given by

$$I_d(x,t)=\begin{cases} b, & 0\le x\le \dfrac{T-t}{2} \\ b-\dfrac{b-c}{t}\left(x-\dfrac{T-t}{2}\right), & \dfrac{T-t}{2}\le x\le \dfrac{T+t}{2} \\ c, & \dfrac{T+t}{2}\le x\le T \end{cases}$$

$$I_a(x,t)=\begin{cases} a, & 0\le x\le \dfrac{T-t}{2} \\ a+\dfrac{d-a}{t}\left(x-\dfrac{T-t}{2}\right), & \dfrac{T-t}{2}\le x\le \dfrac{T+t}{2} \\ d, & \dfrac{T+t}{2}\le x\le T \end{cases} \quad (4)$$

The assumption of transitions taking place in the middle of the window simplifies solution of the equation. The resulting equations are also valid for transitions taking place elsewhere in the window because the sum of ''all'' possible products between $I(x,t)$ and $I(x,t+\tau)$ does not change by shifting the location of transition. Inserting these values for $I_a(x,t)$ and $I_d(x,t)$ into Eq. 2 gives

$$CC_{\tau<t}(\tau,t)\approx -\frac{2(d-a)(b-c)}{3t^2T(a+d)(b+c)}\tau^3+\frac{2(d-a)(b-c)}{tT(a+d)(b+c)}\tau^2 +\frac{2(ac-ab-bd-dc)}{T(a+d)(b+c)}\tau+\frac{2(d-a)(b-c)t}{3T(a+d)(b+c)} +\frac{2(ab+cd)}{(a+d)(b+c)}-1 \quad (5)$$

$$CC_{t\le\tau\le\frac{T-t}{2}}(\tau,t)=\frac{4(ac-ab-cd)}{(T-\tau)(a+d)(b+c)}\tau +\frac{2(ab+cd)T}{(T-\tau)(a+d)(b+c)}-1. \quad (6)$$

We need to get an averaged correlation from multiple FRET traces, as the cross correlation from a single FRET trace is too noisy to fit to Eq. 5 or Eq. 6. To get an analytical solution of an averaged correlation, a single folding intermediate is assumed. According to this assumption, individual folding transition times should be exponentially distributed, which gives the averaged cross correlation of

$$CC(\tau,t)\approx\frac{\int_r^\tau e^{-t'/t}CC_{t'\le\tau\le\frac{T-t}{2}}(\tau,t')dt'+\int_\tau^T e^{-t'/t}CC_{\tau<t'}(\tau,t')dt'}{\int_r^T e^{-t'/t}dt'}, \quad (7)$$

where r is the shortest measurable interval between photons and t is the decay time in the exponential distribution of folding times. Incorporating Eqs. 5 and 6 into Eq. 7, making an approximation to a third-order polynomial, and separating into early and late time regimes yield

$$\approx\begin{cases} C_3\tau^3+C_2\tau^2+\dfrac{2(ac-ab-bd-dc)}{T(a+d)(b+c)}\tau+\dfrac{2(d-a)(b-c)t}{3T(a+d)(b+c)}+\dfrac{2(ab+cd)}{(a+d)(b+c)}-1 & (\tau<t\ll T) \\ \dfrac{\int_\tau^T e^{-t'/t}CC_{\tau<t'}(\tau,t')dt'}{\int_r^T e^{-t'/t}dt'}+\dfrac{4(ac-ab-cd)(1-e^{-\frac{\tau}{t}})}{T(a+d)(b+c)}\tau+\dfrac{2(ab+cd)}{(a+d)(b+c)}-1 & (t\le\tau\ll T) \end{cases}$$

$$C_3=-\frac{2(d-a)(b-c)\int_\tau^T\frac{e^{-t'/t}}{t'^2}dt'}{3T(a+d)(b+c)\int_r^T e^{-t'/t}dt'},\quad C_2=\frac{2(d-a)(b-c)\int_\tau^T\frac{e^{-t'/t}}{t'}dt'}{T(a+d)(b+c)\int_r^T e^{-t'/t}dt'}. \quad (8)$$

Intensity variations caused by environmental heterogeneity do not alter Eq. 8, provided that FRET efficiencies remain unchanged. This is because all the denominators and numerators in Eq. 8 are composed of the same order of intensity terms. By assuming FRET transition is from ~0 to ~1 and the total fluorescence count of donor and acceptor stays constant before and after the transition, Eq. 8 further simplifies to Eq. 9 where A and B are the FRET efficiencies before and after the transition, respectively.

$$\approx\begin{cases} C_3\tau^3+C_2\tau^2+\dfrac{2(A^2-2AB-B^2)}{T(A+B)^2}\tau+\dfrac{2(A-B)^2t}{3T(A+B)^2}+\dfrac{4AB}{(A+B)^2}-1 & (\tau<t\ll T) \\ \dfrac{\int_\tau^T e^{-t'/t}CC_{\tau<t'}(\tau,t')dt'}{\int_r^T e^{-t'/t}dt'}+\dfrac{4(A^2-2AB)(1-e^{-\frac{\tau}{t}})}{T(A+B)^2}\tau+\dfrac{4AB}{(A+B)^2}-1 & (t\le\tau\ll T) \end{cases}$$

$$C_3=-\frac{2(A-B)^2\int_\tau^T\frac{e^{-t'/t}}{t'^2}dt'}{3T(A+B)^2\int_r^T e^{-t'/t}dt'},\quad C_2=\frac{2(A-B)^2\int_\tau^T\frac{e^{-t'/t}}{t'}dt'}{T(A+B)^2\int_r^T e^{-t'/t}dt'}. \quad (9)$$

Note that the intercept of Eq. 9 in $\tau < t \ll T$ depends on A and B, which are experimentally determined, T, which is known exactly, and the average transition time t. Thus, only the intercept is accurately required to analytically determine the folding time. In case of multiple intermediate steps during the folding, transition time t in the intercept of Eq. 9 ($\tau < t \ll T$) becomes the sum of all intermediate state lifetimes during the folding process, because the terms in convolution (Eq. 7) will simply become multiple integrals over independent variables. Therefore, the folding process time determined from the intercept of Eq. 9 ($\tau < t \ll T$) is the total folding process time regardless of the number of intermediate states.

In practice, single photon traces always include background photons, and the background cannot be corrected since the origin of an individual photon is unknown. Indeed, conventional intensity analysis cannot be used if it requires direct background correction. When Eq. 9 is used with FRET values from traces with background, A and B should be replaced with $A' - n/I_{\text{tot}}$ and $B' - n/I_{\text{tot}}$, respectively, where A' and B' are FRET values with background, n is the number of background photons in one channel, and I_{tot} is the total number of photons. In practice, n/I_{tot} can be determined by using Eq. 9 in $t \leq \tau \ll \text{T}$, and fitting the correlation curve to a line within a proper time range. With the background corrected A and B, we determine the intercept of the correlation and use Eq. 9 ($\tau < t \ll T$) to measure folding transition time t. Although the individual intercepts depend on different background levels, the difference between them does not. Therefore, this method measures the transition time as a difference between the instantaneous correlations of two different time regions ($t \leq \tau \ll \text{T}$ and $\tau < t \ll T$). Note that, since FRET efficiencies are used in the analysis, slight variations in individual dye intensities do not alter the results significantly. To determine the intercept of the correlation, we fit the correlation to a third-order polynomial in the range of $\tau <$ t. We fix the first order coefficient from the background-corrected A and B to lower the fitting error.

To determine the precision and accuracy of the method, simulations were performed to randomly produce photons during a FRET transition of predetermined transition time, t_{TRUE}. The validity of simulation is confirmed as in Fig. 2. Single molecule cross correlations were calculated from the individual simulated photon traces of exponentially distributed folding times with the decay time of t_{TRUE}. The average of all single molecule cross correlations was then fit with Eq. 9 ($\tau < t \ll T$) to find the transition time, t_{FIT}, which was compared to t_{TRUE} to determine the error of the fit (Fig. 3). Average photon emission rate of donor, the window size, T, and t_{TRUE} were varied independently to determine the significance of each of these parameters (Fig. 3). Several important points regarding the confidence level of the measured transition time are confirmed or revealed by these simulations.

To explain the findings from the simulations, we must discuss the noise involved in the correlation. Assuming the only source of noise is Poissonian photon emission, the propagated noise to cross correlation is approximated to

$$\sigma_{\text{cc}}(\tau, \Delta\tau) = \frac{2}{\sqrt{(T-\tau)Np(1-A)Bf(\tau, \Delta\tau)}}, \qquad (10)$$

where A and B are the background noncorrected FRET efficiencies before and after the transition, respectively, T is

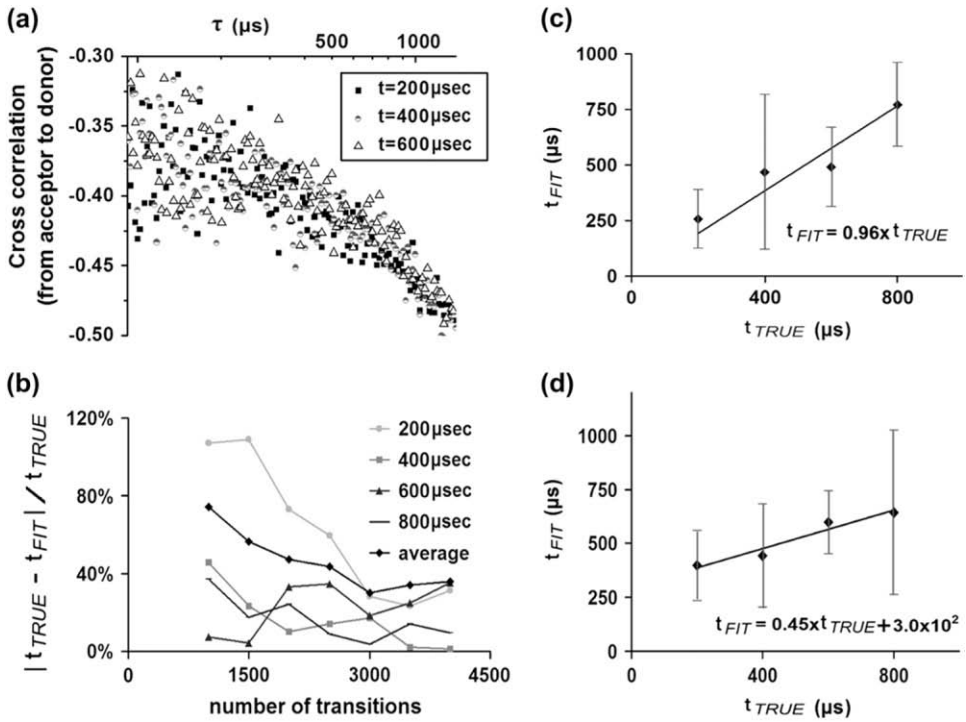

FIGURE 3 Simulated cross correlations based on the model in Fig. 2, fitting errors, and calibration curves. (*a*) Averaged cross correlations with single exponentially distributed transition times with $t_{\text{TRUE}} = 200$, 400, and 600 μs. Three-thousand transitions are averaged per each case with 5 kHz photon emission rate, $A = 0.2$, $B = 0.8$, and $T = 10$ ms. As t_{TRUE} increases, the intercept of the cross-correlation curve becomes more positive (i.e., the triangular points are above the squares and the circles in the small τ region). (*b*) Error between t_{FIT} and t_{TRUE} with respect to the number of simulated transitions averaged. Each data point is averaged from four to 10 cases. (*c*) A calibration curve to correct the error in t when correlations from 3000 transitions are averaged. Points were averaged from four to 10 cases. Standard deviation at each point is also shown in the chart. In the range of 200–800 μs, the t_{FIT} estimates t_{TRUE} reasonably well (within an average error of 30%). (*d*) A calibration curve in the case of 1000 transitions averaged.

the size of data window, N is the number of transitions averaged, p is the photon emission rate including background, and $f(\tau,\Delta\tau)$ is the probability of detecting multiple photons during $\tau \sim \tau + \Delta\tau$ with given p; $f(\tau,\Delta\tau)$ can be straightforwardly obtained from Poisson statistics. Equation 10 is plotted as in Fig. 4 and the photon emission rate of the experiments can be estimated by fitting the plot. The average difference in the cross correlation (ΔCC) between cases with $t = 0$ and $t \neq 0$ in the fitting range can be calculated using Eq. 9. The average noise in the difference of the two cases in the fitting range can be approximated to

$$Noise\ in\ \Delta CC(\tau) = \frac{\sqrt{2}\sum_{i}^{n}\sigma_{cc}(\tau_i, \tau_{i+1} - \tau_i)}{n\sqrt{n}}, \qquad (11)$$

where n is the number of fitting points. The ratio of ΔCC to Eq. 11 (i.e., signal/noise) is equivalent to the t-value of the "t-test".

We started the analysis on our experimental data with 200 ms aperture width (i.e., $T = 200$ ms) to find that the aperture size is too wide to resolve the timescale of the transitions under our experimental conditions. The noise of ΔCC is approximately proportional to $1/\sqrt{T}$ (from Eq. 10) whereas ΔCC is approximately proportional to $1/T$, yielding $1/\sqrt{T}$ dependence in confidence level of the fitting. Thus, by narrowing the correlation window size T, we can get better confidence level by the factor of square root of the window size ratio. However, too narrow T gives too high noise level in the long-time regime, which makes it difficult to estimate the background from Eq. 9 ($t \leq \tau \ll$ T). From the simulation, with a 5-kHz photon emission rate, 10 ms is found to be the narrowest usable window size among the time windows examined. A comparison of simulations with a window of 5, 10, and 25 ms revealed that significantly less transitions are required for the same accuracy in fitting data from the 10-ms window compared to the 5- and 25-ms windows. For example, to measure a 200-μs transition time with a 10-ms window requires only 1000 transitions, whereas 1500 transitions was not sufficient for the 5- or 25-ms window.

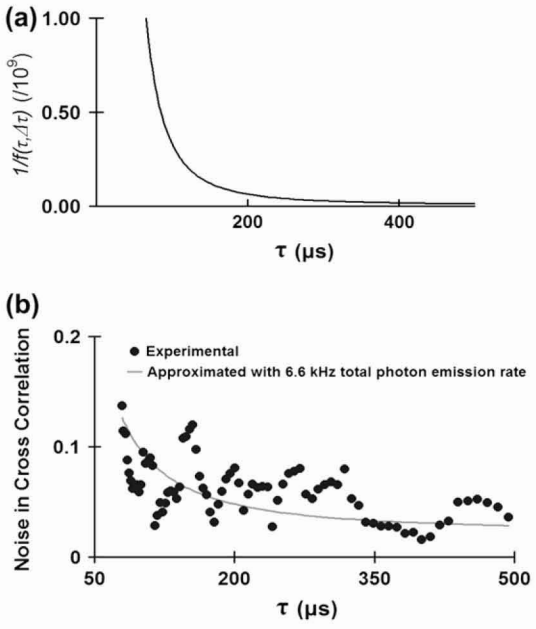

FIGURE 4 Noise in the cross correlation. (*a*) Reciprocal probability of detecting multiple photons within $\tau \sim \tau + \Delta\tau$ as in Eq. 10, i.e., the Poissonian noise in the correlation. (*b*) Noise of experimental data fitted to Eq. 11. Experimental conditions are $A = 0.344$, $B = 0.747$, $T = 10$ ms, and $N = 1133$. Least square fit estimates 6.6 kHz as the average photon emission rate including background.

The other practical point confirmed from the simulation is that too small τ region of data is detrimental to the confidence of results because of the high noise level. The error increases approximately exponentially as τ decreases (Fig. 4 *a*). Because ΔCC between $t = 0$ and $t \neq 0$ is well approximated to a third-order polynomial and $\Delta CC(0)$ with $t \leq$ 800 μs is at most comparable to the average noise level of the correlation, there should be a point in τ in Fig. 4 where the noise starts dominating ΔCC as τ gets smaller. It will, thus, diminish the accuracy of the results to include too early time points. The earliest τ to be included in the fitting should be optimized considering the accuracy of the method and the shortest measurable t. To achieve the highest confidence in the result, the earliest τ of the fitting range was determined by comparing t_{TRUE} to t_{FIT} from simulations. We determined 80 μs was the earliest fitting point to yield t_{TRUE} from t_{FIT} with the best confidence level for t_{TRUE} = 200–800 μs.

Because Eq. 9 is only correct for $\tau <$ t, the following procedure was used to determine the upper limit of fitting. Multiple test fittings were done per averaged correlation by setting each time point in the entire data as the upper limit of fitting (the lower limit of fitting is always 80 μs). Five consecutive time points with the minimum discrepancy between the upper limit (i.e., the time point) and the measured transition time were identified, and the median time was chosen as the upper limit. By using these methods to fit the experimental cross correlation (Fig. 5) to a third-order polynomial, the folding transition time was found to be 440 μs in the fitting range of 80–594 μs. For comparison, the unfolding time is found to be too short to measure with this method (Fig. 5 *b*). Because the experimental conditions and analysis were the same for both folding and unfolding transitions, the significant difference in measured rates is evidence of the validity of this method.

Although the sample includes ~20% of contaminants that could have somewhat different properties than the bulk (see Materials and Methods), the measurement is valid because the signal of interest dominates the contamination; i.e., the number of contaminating molecules (~200) is far less than the required number of molecules (~1000) to yield any significant difference in the correlation. Nevertheless, there appears to be a systematic bias in t_{FIT} particularly for fairly small numbers of transitions (<2000). The discrepancy

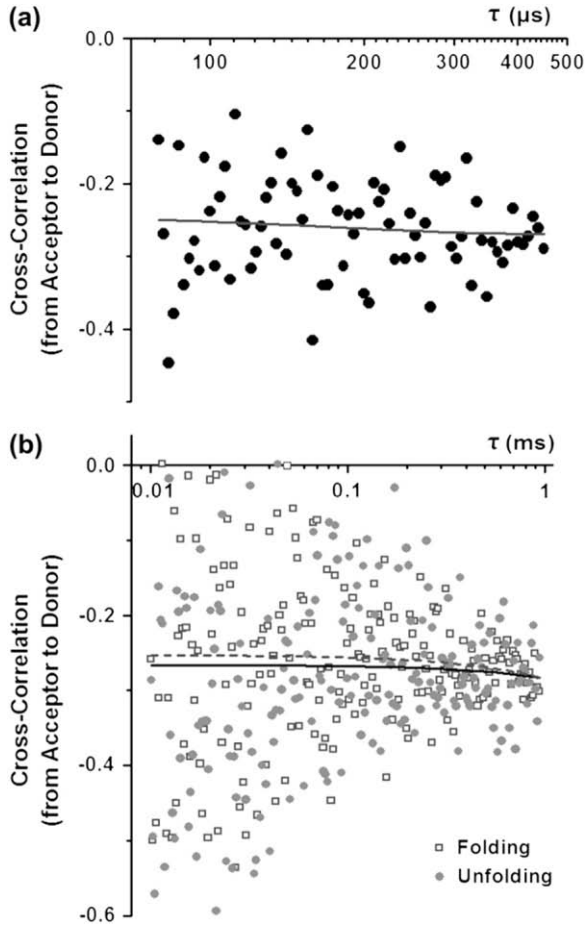

FIGURE 5 Averaged cross correlations of photons from folding and unfolding events. (*a*) An average cross correlation from 1133 folding events with the 10-ms data window around the folding. Average photon emission rate from the dye is ~5 kHz. FRET efficiencies before and after the transitions from Fig. 1 *d* were shifted to correct the background. To correct the background, data in the range from 400 μs to 1 ms are fit to a line, giving an intercept of −0.245, thereby $A' - n/I_{tot}$ and $B' - n/I_{tot}$ are found to be 0.205 and 0.608, respectively. The data were fitted to a third-order polynomial to yield folding time of 310 μs from Eq. 9 and calibration curve in Fig. 3 *d*. Accounting the difference in total number of photons before and after the transition, the folding time is further corrected to 240 μs. (*b*) Comparison between the cross correlation of folding transitions in panel *a* and the averaged cross correlation from 1202 unfolding transitions with $T = 10$ ms. Cross correlation from unfolding transition is shifted upward to cancel out the effect of different background level by matching the two correlation curves in the region from 400 μs to 1 ms. The unfolding transition time is found to be too short to measure with the proposed method. The two correlations show apparent difference in their short time regime (<400 μs), with more positive correlation values for the folding transition. The solid and dashed lines are linear fits to the correlations for unfolding and folding, respectively, to clearly show the difference in the early time region correlation. The intercept of the correlation from the unfolding transition is significantly different from the folding transition and yields a transition time too short to measure with the current method. Therefore, this unfolding transition time can serve as an experimental control.

between t_{FIT} and t_{TRUE} determined from simulations of 1000 transitions (Fig. 3 *d*) was used to correct the fitted t of the data in Fig. 5. Accordingly, the folding time of 440 μs determined from the fitting as described above (Fig. 5 *a*) is adjusted to 310 μs. The average ΔCC for $t = 310$ μs in the range of 80–310 μs is 0.0221 from Eq. 9. Using the approximated error in Fig. 4 *b*, signal/noise in ΔCC (ΔCC divided by Eq. 11) in the fitting range of 80–310 μs with $T = 10$ ms, $p = 6.6$ kHz, $N = 1133$, and $n = 59$ (as in our data, $\tau_{i+1} = \tau_i \times 10^{0.01}$) is 1.767 (Eq. 11). Because ΔCC is always positive, this value corresponds to 94% confidence level in the fitting.

Finally, the assumption of constant total counts before and after the transition introduces an error because we have ~23% more photons after the transition. By using Eq. 8, for the case of a 0.403 FRET change, a 23% increase in the total number of photons after the transition was found to introduce 24% overestimation in the transition time from the intercept. The error in calculating the first order coefficient in Eq. 9 with this assumption was neglected because it is too small (<1%) to significantly affect our accuracy level. Therefore, to compensate the overestimation from this nonconstant total counts, the folding time is corrected to 240 μs.

DISCUSSION

We have presented a method to measure an RNA folding transition time on the single molecule level. We have tested the method on the P4–P6 domain of the *Tetrahymena* group I intron ribozyme. Previous measurements of immobilized molecules using integrative photon counting have had the time resolution only to measure the dwell time in steady states (5,30), but not the transition times between states that appear instantaneous on the millisecond timescale. In this study we have used FCS only on photons detected within 10 ms of a transition between FRET states and have fitted the correlation to the proposed model to yield the average folding transition time of 240 μs.

Although this folding time is significantly faster than any process previously measured in P4–P6 and is one of the fastest measurements made on the single molecule level, it is nevertheless a very noisy measurement and the error in 200–400 μs transition time is ~40–50%. This is due to the inherently long dwell time (~3 s) in the steady states and the experimentally low photon counting rate set by the power of the excitation laser so that at least one transition was detected before photobleaching. This method would be more effective in a system that had an inherently shorter dwell, but dwell times need to be at least 50 ms so that each transition can be isolated in a 10-ms window. Raising the photon counting rate may raise this limit by allowing for shorter windows, but only if the photobleaching rate is not so high that it prevents collection of adequate amounts of data.

This new method measures the transition time between stable folding states on the single molecule level for times as

short as the average photon arrival interval. However, due to the photon emission rate of our fluorophores, in this work we could only resolve the total transition time and not any intermediate steps. Nevertheless, this method provides information about the folding transition that cannot be obtained by more traditional stopped-flow methods that typically operate on the millisecond timescale. It should be interesting to compare this method with folding rates measured by faster mixing methods (31,32) because folding prompted by a large change in Mg^{2+} ion concentration may not duplicate folding in equilibrium.

The $[Mg^{2+}]$ in our experiments was chosen to ensure the maximum number of folding/unfolding transitions. The window of such $[Mg^{2+}]$ is too narrow to make it practical to use $[Mg^{2+}]$ as an experimental control. The strength of this particular system is that it illustrates the core idea of the article: it is possible to squeeze information out of single photons by time-aperturing photon stream.

The microsecond transition may represent one of the following: i), the lifetime of an intermediate mid-FRET state after leaving the low FRET state (33) or, ii), the kinetic time it takes to transition from the low FRET state to a compact, high FRET state, which may or may not be the fully folded state because the FRET probes cannot distinguish between the fully folded state and a highly compact partially unfolded state. It will be informative to use varied conditions and mutants to probe the nature and properties of this now-accessible transition. Future development of brighter fluorescence probes may further increase the information content of this approach, revealing details of the folding transition.

This work was supported by National Science Foundation (PHY-0420752 to Steven Chu) and National Institutes of Health (P01 GM66275-01A1RV to Steven Chu and Dan Herschlag). The research of Lisa Lapidus, PhD. was supported in part by a Career Award at the Scientific Interface from the Burroughs Wellcome Fund.

REFERENCES

1. Ha, T., I. Rasnik, W. Cheng, H. P. Babcock, G. H. Gauss, T. M. Lohman, and S. Chu. 2002. Initiation and re-initiation of DNA unwinding by the Escherichia coli Rep helicase. *Nature*. 419:638–641.
2. Weiss, S. 2000. Measuring conformational dynamics of biomolecules by single molecule fluorescence spectroscopy. *Nat. Struct. Biol.* 7: 724–729.
3. Babcock, H., X. W. Zhuang, R. Russell, L. Bartley, D. Herschlag, and S. Chu. 2001. A single molecule study of the folding dynamics of a large RNA enzyme. *Biophys. J.* 80:201A. (Abstr.).
4. Zhuang, X., L. E. Bartley, H. P. Babcock, R. Russell, T. Ha, D. Herschlag, and S. Chu. 2000. A single-molecule study of RNA catalysis and folding. *Science*. 288:2048–2051.
5. Kim, H. D., G. U. Nienhaus, T. Ha, J. W. Orr, J. R. Williamson, and S. Chu. 2002. Mg^{2+}-dependent conformational change of RNA studied by fluorescence correlation and FRET on immobilized single molecules. *Proc. Natl. Acad. Sci. USA*. 99:4284–4289.
6. Tan, E., T. J. Wilson, M. K. Nahas, R. M. Clegg, D. M. J. Lilley, and T. Ha. 2003. A four-way junction accelerates hairpin ribozyme folding via a discrete intermediate. *Proc. Natl. Acad. Sci. USA*. 100:9308–9313.
7. Margittai, M., J. Widengren, E. Schweinberger, G. F. Schroder, S. Felekyan, E. Haustein, M. Konig, D. Fasshauer, H. Grubmuller, R. Jahn, and C. A. M. Seidel. 2003. Single-molecule fluorescence resonance energy transfer reveals a dynamic equilibrium between closed and open conformations of syntaxin 1. *Proc. Natl. Acad. Sci. USA*. 100:15516–15521.
8. Cosa, G., E. J. Harbron, Y. Zeng, H.-W. Liu, D. B. O'Connor, C. Eta-Hosokawa, K. Musier-Forsyth, and P. F. Barbara. 2004. Secondary structure and secondary structure dynamics of DNA hairpins complexed with HIV-1 NC protein. *Biophys. J.* 87:2759–2767.
9. Magde, D., E. Elson, and W. W. Webb. 1972. Thermodynamic fluctuations in a reacting system-measurement by fluorescence correlation spectroscopy. *Phys. Rev. Lett.* 29:705–708.
10. Elson, E. L., and D. Magde. 1974. Fluorescence correlation spectroscopy. I. Conceptual basis and theory. *Biopolymers*. 13:1–27.
11. Borsch, M., P. Turina, C. Eggeling, J. R. Fries, C. A. M. Seidel, A. Labahn, and P. Graber. 1998. Conformational changes of the H^+-ATPase from Escherichia coli upon nucleotide binding detected by single molecule fluorescence. *FEBS Lett.* 437:251–254.
12. Aragon, S. R., and R. Pecora. 1975. Fluorescence correlation spectroscopy and Brownian rotational diffusion. *Biopolymers*. 14:119–137.
13. Haupts, U., S. Maiti, P. Schwille, and W. W. Webb. 1998. Dynamics of fluorescence fluctuations in green fluorescent protein observed by fluorescence correlation spectroscopy. *Proc. Natl. Acad. Sci. USA*. 95:13573–13578.
14. Widengren, J., J. Dapprich, and R. Rigler. 1997. Fast interactions between Rh6G and dGTP in water studied by fluorescence correlation spectroscopy. *Chem. Phys.* 216:417–426.
15. Yang, H., and X. S. Xie. 2002. Statistical approaches for probing single-molecule dynamics photon-by-photon. *J. Chem. Phys.* 117: 10965–10979.
16. Bonnet, G., O. Krichevsky, and A. Libchaber. 1998. Kinetics of conformational fluctuations in DNA hairpin-loops. *Proc. Natl. Acad. Sci. USA*. 95:8602–8606.
17. Kruger, K., P. J. Grabowski, A. J. Zaug, J. Sands, D. E. Gottschling, and T. R. Cech. 1982. Self-splicing RNA: autoexcision and autocyclization of the ribosomal RNA. *Cell* 31:147–57.
18. Herschlag, D., and T. R. Cech. 1990. DNA cleavage catalyzed by the ribozyme from Tetrahymena. *Nature*. 344:405–409.
19. Doherty, E. A., and J. A. Doudna. 1997. The P4–P6 domain directs higher order folding of the Tetrahymena ribozyme core. *Biochemistry*. 36:3159–3169.
20. Deras, M. L., M. Brenowitz, C. Y. Ralston, M. R. Chance, and S. A. Woodson. 2000. Folding mechanism of the Tetrahymena ribozyme P4–P6 domain. *Biochemistry*. 39:10975–10985.
21. Silverman, S. K., M. L. Deras, S. A. Woodson, S. A. Scaringe, and T. R. Cech. 2000. Multiple folding pathways for the P4–P6 RNA domain. *Biochemistry*. 39:12465–12475.
22. Lehnert, V., L. Jaeger, F. Michel, and E. Westhof. 1996. New loop-loop tertiary interactions in self-splicing introns of subgroup 1C and ID: a complete 3D model of the Tetrahymena thermophila ribozyme. *Chem. Biol.* 3:993–1009.
23. Russell, R., I. S. Millett, S. Doniach, and D. Herschlag. 2000. Small angle X-ray scattering reveals a compact intermediate in RNA folding. *Nat. Struct. Biol.* 7:367–370.
24. Silverman, S. K., and T. R. Cech. 1999. RNA tertiary folding monitored by fluorescence of covalently attached pyrene. *Biochemistry*. 38:14224–14237.
25. Rangan, P., B. Masquida, E. Westhof, and S. A. Woodson. 2003. Assembly of core helices and rapid tertiary folding of a small bacterial group I ribozyme. *Proc. Natl. Acad. Sci. USA*. 100:1574–1579.
26. Forster, T. 1959. Transfer mechanisms of electronic excitation. *Discuss. Faraday Soc.* 27:7–17.
27. Moore, M. J., and P. A. Sharp. 1992. Site-specific modification of pre-mRNA: the 2′-hydroxyl groups at the splice sites. *Science*. 256:992–997.
28. Basu, S., R. P. Rambo, J. Strauss-Soukup, J. H. Cate, A. R. Ferre-D'Amare, S. A. Strobel, and J. A. Doudna. 1998. A specific monovalent

metal ion integral to the AA platform of the RNA tetraloop receptor. *Nat. Struct. Biol.* 5:986–992.

29. Widengren, J., and P. Schwille. 2000. Characterization of photoinduced isomerization and back-isomerization of the cyanine dye Cy5 by fluorescence correlation spectroscopy. *J. Phys. Chem. A.* 104:6416–6428.
30. Katiliene, Z., E. Katilius, and N. W. Woodbury. 2003. Single molecule detection of DNA looping by NgoMIV restriction endonuclease. *Biophys. J.* 84:4053–4061.
31. Brody, J. P., P. Yager, R. E. Goldstein, and R. H. Austin. 1996. Biotechnology at low Reynolds numbers. *Biophys. J.* 71:3430–3441.
32. Hertzog, D. E., X. Michalet, M. Jäger, X. Kong, J. G. Santiago, S. Weiss, and O. Bakajin. 2004. Femtomole mixer for microsecond kinetic studies of protein folding. *Anal. Chem.* 76:7169–7178.
33. Jung, J., and A. VanOrden. 2006. A three-state mechanism for DNA hairpin folding characterized by multiparameter fluorescence fluctuation spectroscopy. *J. Am. Chem. Soc.* 128:1240–1249.